Educational Administration: Theory and Practice
2024, 30(1), 3065-3081
ISSN: 2148-2403
https://kuey.net/

Research Article

A Five Level Inverter With Three Tyre Meta-Heuristic Aware Optimal Parameter Selection

B Mohan Rao[1*], Md. Haseeb Khan[2], B. Mangu[3]

[1*]Department of Electrical Engineering, University College of Engineering (A), Osmania University, Hyderabad, India.
[2]Muffakham Jah college of Engineering and Technology, Osmania University, Hyderabad, India.
[3]Department of Electrical Engineering, University College of Engineering (A), Osmania University, Hyderabad, India.

***Corresponding Author:** B Mohan Rao
*E-mail: bodamohan1@gmail.com

Citation: B Mohan Rao et al (2024), A Five Level Inverter With Three Tyre Meta-Heuristic Aware Optimal Parameter Selection., *Educational Administration: Theory and Practice*, *30*(1), 3065-3081
Doi: 10.53555/kuey.v30i1.6981

ARTICLE INFO
Received 02/03/2024
Accepted 12/04/2024

ABSTRACT

In recent years, Multi-Level Inverters (MLIs) have gained significant traction in industrial and grid-connected settings owing to their numerous benefits. To enhance the efficiency of grid-connected PV systems employing five-level inverters, three controllers are employed to govern the control process. The control scheme comprises three loops utilizing FOPI, PID, and PI controllers: one for regulating the intermediate circuit voltage (Vdc) and the remaining two for managing the direct and quadratic currents (Ix, Iy) provided by the multilevel inverter. Precise selection of controller parameters (Kp, KI, λ) is imperative to elevate the efficiency of the multi-level inverter while simultaneously reducing the total harmonic distortion (THD) in both voltage and current output. Similarly, optimization of parameters for PID and PI controllers in the Buck converter is carried out to enhance the system's performance. This optimization employs three-level algorithms including Gradient Optimization Algorithms (GOA), Self-Adaptive-Gradient Optimization Algorithms (SA-GOA), and Aquila Improved GOA (AI-GOA). The study evaluates and compares the performance of three controllers: GOA-FOPI, AI-GOA-PID, and SA-GOA-PI, employing various methodologies. The results validate the effectiveness of the proposed system in minimizing THD. The simulation is conducted using MATLAB/Simulink.

Keywords: *Five Level Inverter, Total Harmonic Distortion, Buck converter, Gradient Optimization Algorithm, Aquila Improved GOA.*

1. Introduction

In the last few years, there has been a significant focus on integrating renewable energy sources, especially solar photovoltaic (PV) systems, into the power grid [1]. This attention is driven by increasing concerns about environmental sustainability and the demand for clean energy solutions. Consequently, researchers and engineers have been actively focused on creating new technologies to improve the efficiency, performance, and dependability of solar inverters. Solar inverters play a crucial role in transforming the DC power generated by solar panels into AC power. [2, 3].

However, the quality of power is vital for effective transmission of electricity to consumers because of the changing environmental factors. This is particularly noticeable in solar power generation, where variations in temperature and solar radiation greatly influence the consistency of the electrical output [4]. Solar energy systems are significantly impacted by fluctuations in ambient temperature. Changes in temperature can impact the performance of PV modules, resulting in alterations to the electrical properties of the power produced. Changes in solar irradiance due to factors like cloud cover, time of day, and location can result in fluctuations in the electrical output of PV modules [5, 6]. Therefore, inverter is essential for reducing the effects of temperature variations on power quality and maintaining the stability and dependability of solar energy systems. Their main role involves transforming the direct current produced by solar panels into high-standard AC power that is applicable for residential, commercial, or industrial use [7-9]. Contemporary inverters come with innovative thermal control systems to guarantee efficient performance in varying temperatures. These

mechanisms are vital in preserving the effectiveness of solar power systems and ensuring high-quality electricity supply to connected loads or the grid [10].

Inverters can be equipped with maximum power point tracking (MPPT) algorithms to mitigate fluctuations [11]. MPPT allows the inverter to dynamically adjust the operating point of the PV modules so that the system captures the maximum available power under varying irradiance conditions. [12] This optimization not only increases overall energy output but also helps maintain stable AC voltage and frequency output. Multilevel inverters (MLI) provide enhanced waveform quality by reducing harmonic distortions in the output. Advanced control methods such as predictive control and fuzzy logic offer more precise and adaptable inverter performance [13, 14]. The hybrid inverter systems that integrate solar power with energy storage help to maintain stable power quality by smoothing out fluctuations in solar output through continuous energy supply [15]. However, designing the right inverter technology and control strategies becomes essential for attaining optimal power quality. Due to their many benefits, Multi-Level Inverters (MLIs) have attracted a lot of attention lately, especially in industrial and grid-connected applications. Compared to conventional two-level inverters, these inverters have higher voltage and power capacities, which makes them appropriate for a range of renewable energy systems, such as grid-integrated photovoltaic (PV) systems. Inverter performance and efficiency are crucial to overall energy conversion and grid stability in these kinds of systems. To address the need for improved efficiency and reduced harmonic distortion in grid-connected PV systems employing MLIs, this study proposes a novel approach utilizing a five-level inverter integrated with fractional-order Proportional-Integral (FOPI) controllers. The main objectives of this research are listed below:

- This study proposes the use of fractional order PI (FOPI) controllers for a five-level inverter in a grid-connected PV system. This can improve the efficiency of the system compared to traditional integer order PI controllers.
- The research focuses on optimizing controller parameters (Kp, KI, λ) to enhance the efficiency of the multi-level inverter while simultaneously reducing total harmonic distortion (THD) in both output voltage and current.
- The study employs three different meta-heuristic optimization algorithms (Gradient Optimization Algorithms, Self-Adaptive Gradient optimization algorithms, Aquila improved GOA) to optimize the controller parameters.
- The paper performs a comparison analysis to assess the performance of three alternative controller configurations (GOA-FOPI, AI-GOA-PID, and SA-GOA-PI) in terms of THD reduction.

The remaining of article is organized as follows: The analysis of existing studies is presented in section 2. The proposed model is detailly explained in section 3. The simulation results of proposed system are provided in section 4. Finally, section 5 provides conclusion.

2. Problem statement

The incorporation of solar power into the electric grid poses a significant challenge in maintaining consistent power quality under changing solar irradiance conditions. Variations in solar power output, influenced by factors such as weather and time of day, present a notable risk to the stability and dependability of electric systems. Although existing inverters and control methods are somewhat effective, they often struggle to promptly respond to sudden changes in solar irradiance. This can result in issues like voltage instability, harmonic distortions, and frequency fluctuations that may negatively affect the performance of connected loads and strain the grid's reliability. Overcoming these challenges is crucial for integrating solar power while ensuring power quality standards and grid stability. Therefore, advanced inverter technologies along with effective control methods are required to mitigate the impact of variable solar irradiance on power quality.

3. Proposed Methodology

This study proposed a five level inverter with three tyre meta-heuristic aware optimal parameter selection for various controllers. The PV generators employ all of the transformers. This study employs Buck converter for DC-to-DC converter. The converter is connected to five level inverter of the model through DC link. The overview of proposed model is shown in Fig. 1. The study used three metaheuristic algorithms for control the parameters of three controllers used in this model. The control parameters of FOPI controller are optimized by GOA, parameters of PID controller is optimized using AI-GOA algorithm, and the SA-GOA is used to optimize the parameters of PI controllers.

3.1. Modelling of System

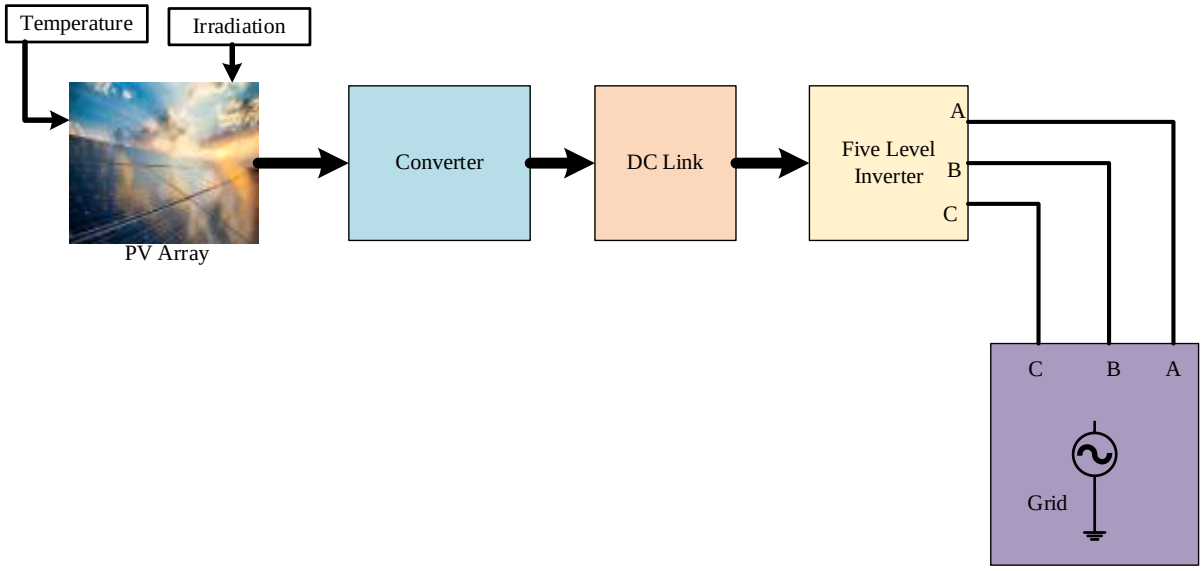

Figure 1: Overview of system model

3.2. Photovoltaic generator

The power modules must be created by connecting these cells in series and parallel due to the extremely limited power that these cells have at their terminals. A photovoltaic module's current-voltage characteristics can be expressed as following Eqn. (1).

$$I = I_{lg} - I_0 \left[exp\left(\frac{u+R_s I}{N_s F k T/q}\right) - 1 \right] - \frac{u+R_s I}{R_{sh}} \quad (1)$$

Where,

$$I_{lg} = \left(I_{lgn} + K_s \Delta T\right) \times \frac{R}{R_n} \quad (2)$$

$$I_0 = \frac{(I_{scn} + K_s \Delta T)}{e^{\left(\frac{V_{ocn}+K_o \Delta T}{N_s F k T/q}\right)}} \quad (3)$$

$$\Delta T = T_a - T_n \quad (4)$$

Where, R_s denotes series resistance, R_{sh} is the shunt resistance, I_{lg} is the light-generated current, I_0 specifies the diode saturation current, N_s indicates the number of series-connected PV cells in the module, F is the diode ideality factor, k is the Boltzmann constant, T is the module temperature, and q is the elementary charge; The cell's nominal irradiance and current are represented by R and R_n, respectively, while the ambient and nominal temperatures are represented by T_a and T_n, short-circuit current under nominal conditions. The open circuit voltage temperature coefficient is indicated by K_o, and the short circuit current coefficient is denoted by K_s. Fig. 1 shows the electrical equivalent circuit of a PV module that corresponds to Eqn. (1). The model is known as the one-diode model. The PV cell is depicted in Figure 1 through the parallel connection of a diode and a current source. The current generated by the light source is exactly proportional to the irradiance. The non-idealities in a PV module are represented by series and shunt resistances.

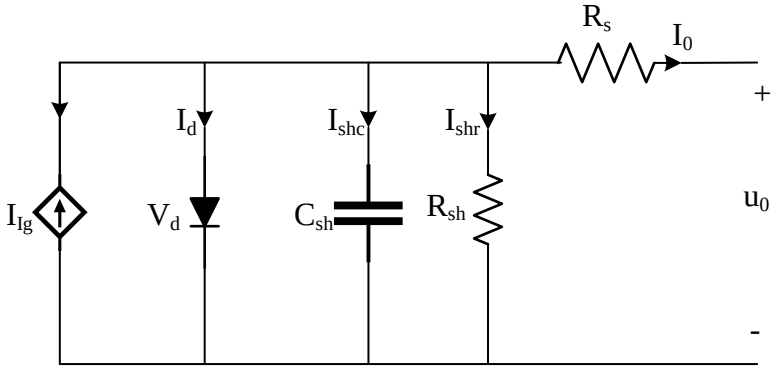

Figure 2: The one-diode equivalent diagram of a PV module.

In Fig. 1, V_d represents the diode's voltage, I_d the diode's current, which includes the diode saturation current and the exponential term in Eqn. (1), I_{sh} specifies the shunt resistance's current, C_{sh} indicates the shunt capacitance, and I_{shc} is the shunt capacitance's current.

3.3. Buck Converter

The DC-DC converter type known as a buck converter, which is depicted in Fig. , is used to step down voltage. It is made up of two energy-storing components, an inductor, and a capacitor, as well as two semiconductor devices, a transistor and a diode. A capacitor is used to lessen output voltage ripple. A combination of an inductor and a capacitor may be utilized in certain situations to reduce load ripple. The state space analysis method was used to support the mathematical modelling of the buck converter since the input and output voltages are predetermined in order to determine the experimental values of the filter component of the buck converter, the inductor, and the capacitor. The buck converter has two modes of operation: 1) ON and 2) OFF for switch. Current enters the load through the inductor in mode 1 when switch is closed. In the end, this process puts diode D in the OFF position by charging the inductor by raising its magnetic field. The diode will show an input supply, and the inductor's current will increase. In the following mode, current passes through the load and diode when the switch is off. The switches and diode regulate the amount of current flowing through the inductor. The current flowing through the inductor is never zero when the buck converter is operating in a continuous mode of conduction. By changing the duty cycle of S1, we may modify the V_{out} to V_{in} ratio. The V_{out} increases with length of time switch is turned on. The expression is provided in Eqn. (5).

$$V_{out} = \frac{T_{ON}}{T} V_{in} \quad (5)$$

Where, V_{in} and V_{out} indicates input and output voltage respectively, T_{ON} is ON time of a switch; T represents switching period.

The output power and the input power will be equal under ideal circumstances. It can be expressed as follows:

$$V_{out} I_{out} = V_{in} I_{in} \quad (6)$$

From Eqn. (5)

$$I_{in} = \frac{T_{ON}}{T} I_{out} \quad (7)$$

Where, I_{in} represents supply current, and I_{out} denotes output current.

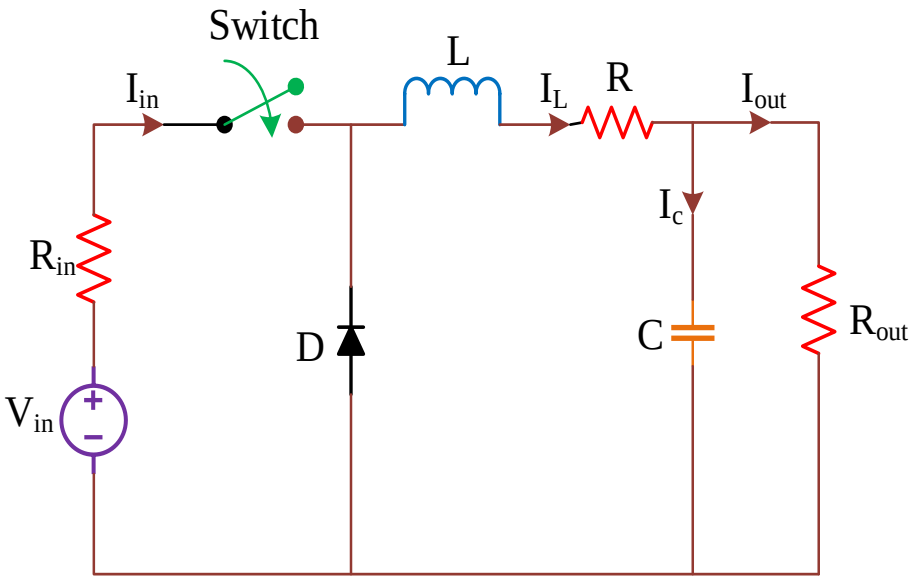

Figure 3: Basic structure of Buck Converter

The fundamental idea behind a buck converter is that input current fluctuations do not occur in the input circuit's inductor. The inductor stores energy as a magnetic field when the switch is ON and releases it when the switch is OFF. It is projected that the output circuit's capacitor is sufficiently large to ensure a high RC circuit time constant in the output stage. A constant output voltage is ensured by the huge time constant about the switching period, $V_{out}(t) = V_{out}(constant)$. The following Eqn. (8) provides the critical inductance (L_c) for the continuous conduction mode:

$$L_c = \frac{(1-D)}{2f} R_{out} \quad (8)$$

The critical capacitance is expressed in following Eqn. (9)

$$C_c = \frac{(1-D)}{16 f^2 L_c} \quad (9)$$

The following Equations can be used to analyse a buck converter:

$$L \frac{dI_L}{dt} = u\, V_{in} - V_{out} \quad (10)$$

$$\frac{dI_L}{dt} = \frac{1}{L}(u\, V_{in} - V_{out}) \quad (11)$$

$$\frac{dV_{out}}{dt} = \frac{1}{C}(I_L - I_{out}) \quad (12)$$

$$I_{out} = \frac{V_{out}}{R_{out}} \quad (13)$$

Where, $u = 1$ for switch ON and $u = 0$ for switch OFF.
Based on the aforementioned equations, Fig. Depicts the mathematical framework of the buck converter.

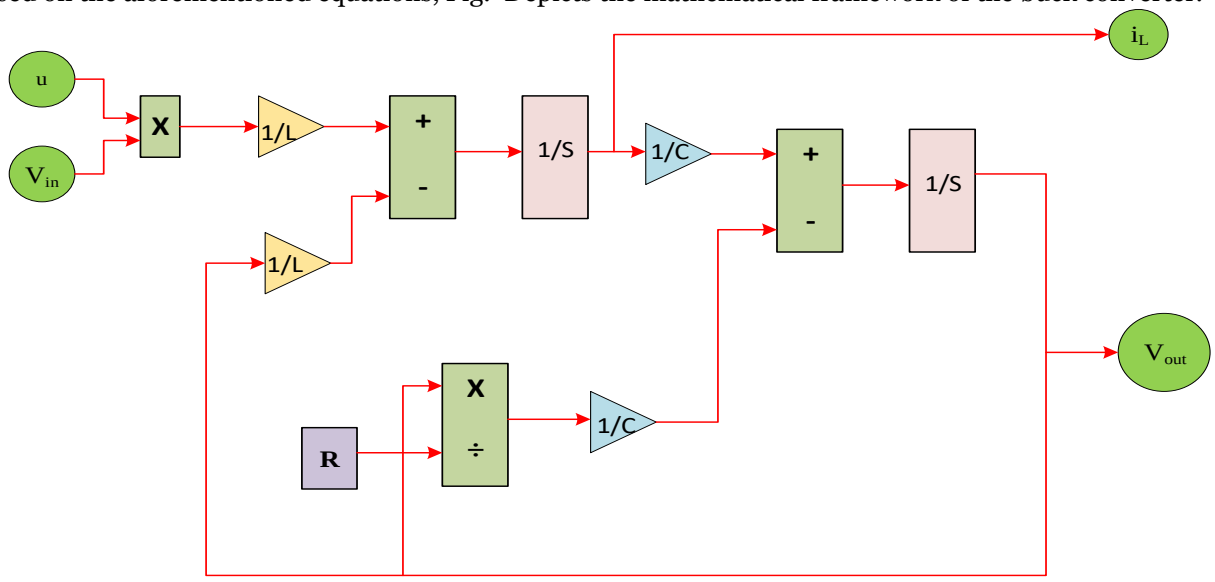

Figure 4: Mathematical model of Buck Converter

3.4. Device linked to Network

The most important part of any grid-connected system is an inverter. The inverter transforms as much Direct Current (DC) power from photovoltaic array as it can into the proper voltage and frequency in order to supply electricity to the grid. The harmonics produced in the sinusoidal signal are eliminated through the use of an LC filter.

3.5. Multilevel Inverter

Minimizing weight, cost, and complexity is necessary for the EV. The system's ability to function properly depends heavily on the torque and speed outputs, which must be tuned. Consequently, the selection of equipment components is crucial, particularly the inverter as it is this device that transforms continuous energy into a different form. Energy waste occurs frequently at this moment. One view of heavy transportation is that it requires a lot of power. An inverter with many levels of voltage is required for this. The sine waveform of the voltage is equivalent to that of the five-level NPC inverter. A better harmonic spectrum may be synthesized by the voltage waveform the more output voltage levels there are. The effectiveness and dependability of the inverter are too crucial to improve behaviour of system. The five-level NPC inverter can choose an output voltage with a low percentage of THD. Since the inverter lowers the THD%, a high switching frequency is necessary. The output quality is also undoubtedly influenced by commutation of switches. In both high and intermediate voltage scenarios, a multi-level inverter arrangement was employed.
The basic construction of this inverter was discussed in Fig. . One of the most popular types of solar systems is the NPC inverter. There are several notable benefits to the system. The multilayer inverter requires the $(n - 1)$ capacitors on DC bus, and $2 \times (n - 1)$ switches are needed for each phase. Furthermore, each phase contains $2 \times (n - 2)$ diodes. The switching state is depicted in Table 2.

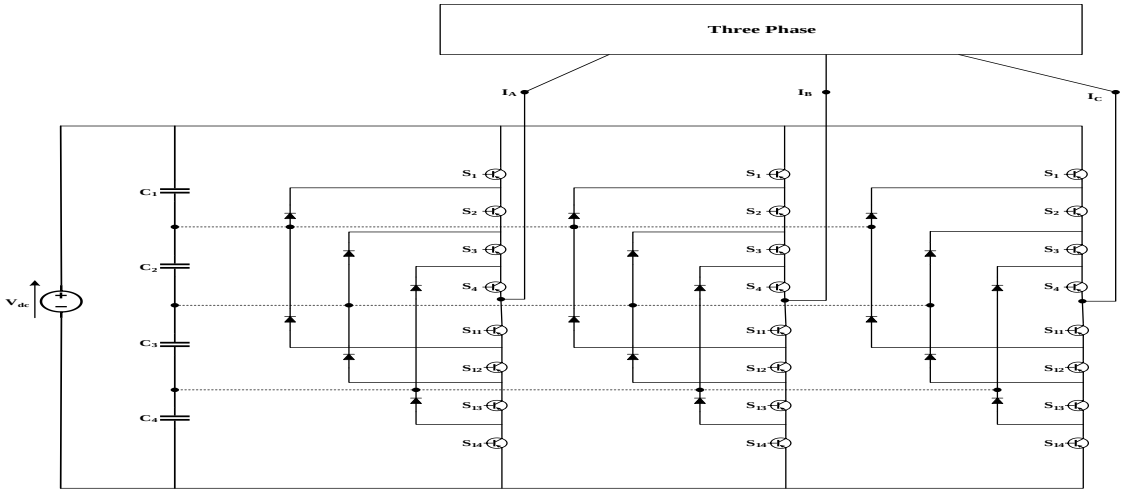

Figure 5: Three phase Five level inverter

Table 2: Switching state of five level inverter

S_1	S_2	S_3	S_4	S_{11}	S_{12}	S_{13}	S_{14}	V_{out}
1	1	1	1	0	0	0	0	$V_{dc}/2$
0	1	1	1	1	0	0	0	$V_{dc}/4$
0	0	1	1	1	1	0	0	0
0	0	0	1	1	1	1	0	$-V_{dc}/4$
0	0	0	0	1	1	1	1	$-V_{dc}/2$

3.6. Control System

The proposed NPC five level inverter features a specific control system designed to facilitate the flow of electricity from the PV generator to the grid. This could only be done by linking a controller. To employ a FOPI controller to guarantee the DC voltage buses' stability within their reference value. As shown in Fig., the output of this FOPI controller will specify the current references and controllers of active currents to the network generated for PV panels.

In this configuration, the current controller loops are discussed. First, the three phase currents (I_A, I_B, and I_C) are converted into two phase currents (x, y). Since we are unable to control the two-phase currents when they are spinning, we further convert them into the two-phase stationary currents (x y), which contain the I_x and I_y currents. I_x and I_y are used to generate the E_x and E_y, which are required to derive the three-phase reference voltages. Grid current is controlled by the constant variables I_x^* and I_y^*. The $D-Q$ axis theory generates I_x and I_y currents from three-phase currents. As illustrated in Fig. PWM can be generated by using E_x and E_y outputs of current controllers as reference voltages. In this operation, the E_x and E_y are transformed into three phase reference voltages: $VAref$, $VBref$, and $VCref$. When the ABC/xy transformation method is applied, the phase-locked loop (PLL) can offer information on grid voltage phase.

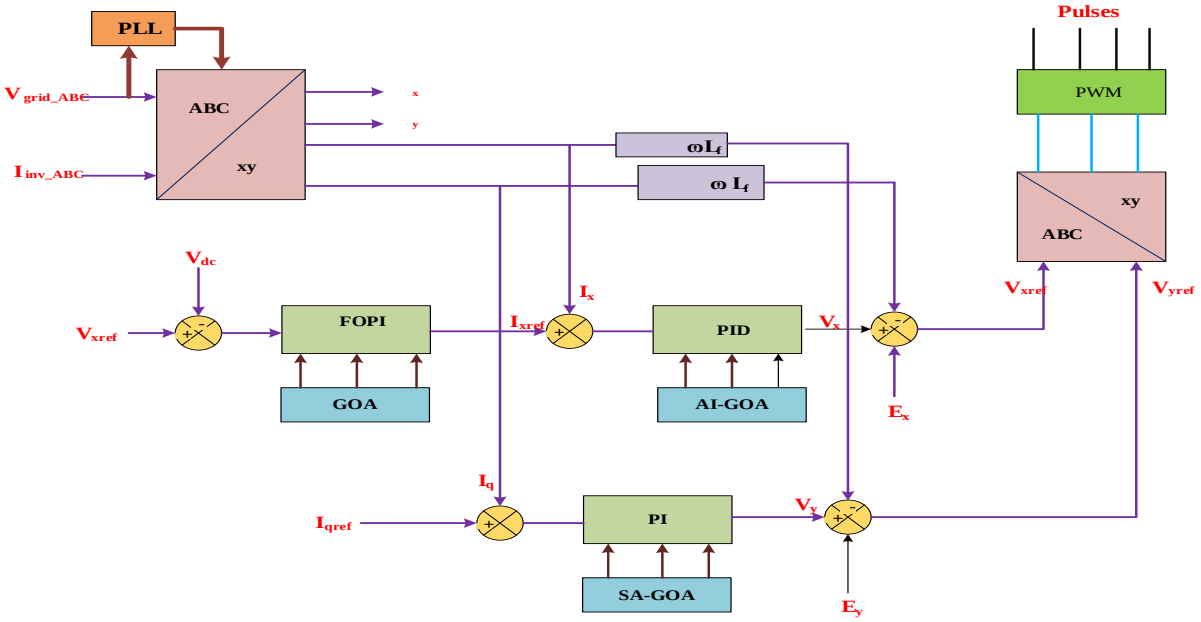

Figure 6: Control diagram

3.6.1. Modulation method

The modulation approach is used in proposed control system. This modulation method employs sine-wave pulse width modulation (SPWM). As illustrated in Fig., a five-level voltage waveform necessitates four level-shifted carrier signals; multiple triangle sinusoidal modulation makes this possible. This method requires (N – 1) triangular signals with the same frequency (fp) and amplitude (Ap). These triangular signals are compared, for each phase, with a reference signal of amplitude ($Aref$) and frequency (Fref). The modulation rate (ma) and frequency ratio (mf) are given in following Eqns. (14) and (15).

$$m_a = A_{ref}/(N-1)A_p \quad (14)$$

$$m_f = \frac{F_p}{F_{ref}} \quad (15)$$

3.6.2. Fractional Order PI (FOPI) Controller

The FOPI controller extends the traditional integer-order PI controller by introducing fractional calculus concepts into its design. The FOPI controller has additional parameters compared to the integer-order PI controller. These parameters typically include the fractional orders (λp, λi) in addition to the proportional gain (Kp) and integral gain (Ki). The fractional orders (λp, λi) allow more flexibility in tuning the controller response, especially in systems with non-integer dynamics or non-linearities.

3.6.3. PI Controller

The Proportional-Integral (PI) controller is a widely used feedback control mechanism in engineering. It consists of two terms: the proportional term, which is proportional to the error signal, and the integral term, which is proportional to the integral of the error signal over time. The PI controller has two main parameters: Kp and Ki, which need to be appropriately tuned to achieve desired system performance.

3.6.4. PID Controller

The Proportional-Integral-Derivative (PID) controller is an extension of the PI controller, which includes a derivative term. The derivative term is proportional to the rate of change of the error signal. In addition to Kp and Ki, the PID controller has a derivative gain (Kd). The inclusion of the derivative term allows the PID controller to anticipate future behaviour based on the current rate of change of the error, improving response time and stability.

3.7. Metaheuristic Algorithm

3.7.1. Gradient Optimization Algorithm (GOA)

Numerous conditions, including optimal power flow, cost-effective load dispatch, estimation of solar PV parameters, controller tuning, and cost-effective emission dispatch, may present difficult tasks. Additionally, different kinds of objectives may be involved, including multiobjective, many-objective, large-scale, and fuzzy optimization. The real-time application necessitates a prompt response whether or not the situation is challenging. Algorithms can be broadly classified into two groups according to their behaviours: algorithms that use accurate information, gradient and sub-gradient information, and slope, and algorithms that employ predicted solutions that are anticipated. The majority have the potential to yield positive outcomes while the efficacy of some of these approaches is unknown.

(i) Initialization phase

The variable α in GOA is regarded as a transformative variable that moves from exploration to exploitation phase. In GOA algorithm, the probability rate is the single control variable. The intricacy of task determines population size S and the number of iterations. GOA consists of S vectors in D-dimensional search space since each member of population is referred to as a vector. The vector has the following expression:

$$Y_{d,y} = \left[Y_{1,y}, Y_{2,y}, \dots, Y_{D,y}\right]$$

$$d = 1,2,\dots.,D \;;\; d = 1,2,\dots.,S \quad (16)$$

In the D-dimensional search space, the beginning position of vector individuals is produced randomly. The similar idea has been stated as follows:

$$Y_y = Y_l + rand(0,1) \times (Y_u - Y_l) \quad (17)$$

Where, the lower and upper bounds of decision variables Y are represented by Y_u and Y_l respectively, and $rand$ stands for random number between [0,1].

(ii) Gradient Search Rule (GSR)

The Gradient Search Rule (GSR), which improves exploration in the promising area, controls vector movements to produce high-quality solutions. The GSR supports GBO in accelerating both the rate of

convergence and the exploration phase. the GSR enables the GBO to fine-tune for random motion to prevent premature convergence and enhance exploration capacity. The Direction of Movement (DM) is a simple way to calculate convergence rate.

$$Y1_y^m = Y_y^m + DM - GSR \quad (18)$$

$$DM = \tau_1 \times rand \times \left(y_b - Y_y^m\right) \quad (19)$$

$$GSR = \tau_1 \times rand_u \times \frac{2\Delta_y \times Y_y^m}{(y_w - y_b + \omega)} \quad (20)$$

The Eqn. (18) is used to update the position of vector; the modified vector is represented by $Y1_y^m$; The symbols m signifies the iteration, τ_1 indicates crucial control variables that maintain balance between exploration and exploitation. The variable ω falls between 0 and 0.1. $rand_u$ denotes uniformly distributed random number. The solutions with most favourable and poorest scores are indicated as y_b and y_w, respectively. The difference between current location and randomly selected position is represented by Δ_y.

$$\tau_1 = 2 \times \alpha \times rand - \alpha \quad (21)$$

$$\alpha = \left|\mu \times sin\left(\frac{3\pi}{2} + sin\left(\frac{3\pi}{2} \times \mu\right)\right)\right| \quad (22)$$

$$\mu = (\mu_{max} - \mu_{min}) \times \left(1 - \left(\frac{i}{i_{max}}\right)^3\right)^2 + \mu_{min} \quad (23)$$

Where, μ_{min} = 0.2, μ_{max} = 1.2, and i_{max} indicates the maximum number of iterations.

$$\Delta_y = |step| \times rand(1: S_p) \quad (24)$$

$$step = \frac{\beta + (y_b - y_{r1}^m)}{2} \quad (25)$$

The parameter β indicates whether the Δ_y is changed during each iteration or not.

$$\beta = rand \times 2 \times \left|\frac{y_{r1}^m + y_{r2}^m + y_{r3}^m + y_{r4}^m}{4} - y_y^m\right| \quad (26)$$

Where, the values are selected at random from [*1, D*] for numbers *r1, r2, r3,* and *r4*. The y_b and y_{r1}^m retrieves the step size $|step|$. τ_2 is the additional random variable that is helpful during the exploration stage. It can be stated as following Eqn.

$$\tau_2 = 2 \times \propto \times rand - \propto \quad (27)$$

The above Eqn. (18) can be rewrite as follows:

$$Y1_y^m = Y_y^m - \tau_1 \times rand_u \times \frac{2\Delta_y \times Y_y^m}{(\omega + XP_y^m - XQ_y^m)} + \tau_2 \times rand \times (y_b - y_{r1}^m) \quad (28)$$

A new population vector $Y2_y^m$ can be expressed as following Eqn. (29)

$$Y2_y^m = y_b - \tau_1 \times rand_u \times \frac{2\Delta_y \times Y_y^m}{(\omega + XP_y^m - XQ_y^m)} + \tau_2 \times rand \times (y_{r1}^m - y_{r2}^m) \quad (29)$$

$$XP_y = rand \times \left(\frac{[Z_{y+1} + y_y]}{2} + \Delta_y \times rand\right) \quad (30)$$

$$XQ_y = rand \times \left(\frac{[Z_{y+1} + y_y]}{2} - \Delta_y \times rand\right) \quad (31)$$

The exploitation step is enhanced by search direction technique. The Eqn. (28) is utilized for global search only, while Eqn. (29) is used to start the local search procedure. To enhance the discovery and exploitation stages, both search procedures have become necessary. The solution $Y3_y^m$ is revised in following iteration based on above-all conversations.

$$Y3_y^m = Y_y^m - \tau_1 \times \left(Y2_y^m - Y1_y^m\right) \quad (32)$$

$$y_y^{m+1} = r_a \times \left(r_b \times Y1_y^m + (1 - r_b) \times Y2_y^m\right) + (1 - r_a) \times Y3_y^m \quad (33)$$

Where, random numbers between [0,1] are represented by the variables r_a and r_b.

(iii) Local Escaping Operator

In GOA, the Local Escaping Operator (LEO) is extremely useful for resolving challenging optimization issues. Through the application of multiple potential solutions, The LEO produces a high-quality solution Y_{LEO}^m by applying solutions like $Y1_y^m$, $Y2_y^m$, y_{r1}^m, y_{r2}^m, y_b, and x_k^m. The following Eqn. (34) is utilized to generate Y_{LEO}^m:

$$Y_{LEO}^{m} = \begin{cases} Y_y^{m+1} + a \times (a_1 \times y_b - a_2 \times x_k^m) + b \times \tau_1 \times \\ \left(a_3 \times \left(Y2_y^m - Y1_y^m\right) + a_2 \times (y_{r1}^m - y_{r2}^m)\right) /2; & if\ rand < 0.5 \\ y_b + a \times (a_1 \times y_b - a_2 \times x_k^m) + b \times \tau_1 \times \\ \left(a_3 \times \left(Y2_y^m - Y1_y^m\right) + a_2 \times (y_{r1}^m - y_{r2}^m)\right) /2; & otherwise \end{cases} \quad (34)$$

Where, a is a uniform random number between [−1, 1], b is a normally distributed random number with mean of 0 and standard deviation of 1. The expression for the random numbers, a_1, a_2, and 3 are as follows.

$$a_1 = Z_1 \times rand \times 2 + (1 - Z_1) \quad (35)$$

$$a_2 = a_3 = Z_1 \times rand + (1 - Z_1) \quad (36)$$

The Z_1 can have a value of either 0 or 1. The Eqn. (34) is used to calculate the solution y_k^m and it can be expressed as follows:

$$y_k^m = \begin{cases} y_{rand}; & if\ u_2 < 0.5 \\ y_p^m; & otherwise \end{cases} \quad (37)$$

$$y_{rand} = Y_l + rand \times (Y_u - Y_l) \quad (38)$$

Where, u_2 represents random number between [0,1], y_{rand} denotes updated solution, and y_p^m indicates the solution of random population. Therefore, the improved version of Eqn. (37) can be stated as follows.

$$y_k^m = Z_2 \times y_p^m + (1 - Z_2) \times y_{rand} \quad (39)$$

Z_1 has a value of either 0 or 1 depending on the value of u_2.

3.7.2. Self-Adaptive Gradient optimization algorithms (SA-GOA)

In many engineering applications, it is essential to adjust the parameters of the PI controller in order to get the desired system behaviour. Traditional trial-and-error techniques are common, but they are not always the best or most efficient. A more methodical approach is provided by gradient-based optimization algorithms; however, fixed learning rates frequently result in slow convergence or local minima stagnation. To solve these issues, this research introduced Root Mean Square Propagation (RMSProp) into GOA to optimize the parameters of PI controller. Simple mini-batch gradient descent or momentum alone cannot be used to train neural networks based on distance measures and Gaussian activation functions. That method cannot achieve any convergence, or only very sluggish convergence. Even in the case of shallow networks, this is true. Applying RMSProp, which makes the training possible in the first place, is the solution. RMSProp has demonstrated outstanding learning rate adaptation across a range of applications.

The learning rate in RMSProp is customized for every parameter vector, c_j^l and r_j^l, where ∀j ∈ {1,...,s_l} and ∀l ∈ {1,..., L}. For every weight, the plan is to maintain a moving average of the squared slopes over nearby mini-batches:

$$\bar{v}\left(c_j^l, t\right) = \delta \bar{v}\left(c_j^l, t-1\right) + (1 - \delta)\left(\partial J / \partial c_j^l\right)^2 \quad (40)$$

$$\bar{v}\left(r_j^l, t\right) = \delta \bar{v}\left(c_j^l, t-1\right) + (1 - \delta)\left(\partial J / \partial r_j^l\right)^2 \quad (41)$$

$$c_j^l = c_j^l - \frac{\eta}{\sqrt{\bar{v}\left(c_j^l, t\right)}} \cdot \partial J / \partial c_j^l \quad (42)$$

$$r_j^l = r_j^l - \frac{\eta}{\sqrt{\bar{v}\left(r_j^l, t\right)}} \cdot \partial J / \partial r_j^l \quad (43)$$

The learning rate parameters of RMSProp is applied in Eqn. (33) and the modified SA-GOA can be expressed in following Eqn. (44).

$$y_y^{m+1} = c_j^l \times \left(r_j^l \times Y1_y^m + \left(1 - r_j^l\right) \times Y2_y^m\right) + \left(1 - c_j^l\right) \times Y3_y^m \quad (44)$$

The key benefits of SA-GOA are described as follows:

- Dynamic learning rates help navigate the search space efficiently, potentially reaching optimal parameters quicker than fixed-rate methods.
- Adapting to the gradient landscape can lead to controllers less susceptible to noise or model uncertainties.
- Adapting learning rates based on individual parameter updates might lead to controllers better handling complex reference signals or system dynamics.

3.7.3. Aquila Improved GOA (AI-GOA)

This section presents the AI-GOA technique which is the combination of Aquila Optimizer and Gradient based optimization algorithm. Optimizing PID controllers is a crucial task in various applications. Traditional methods can be time-consuming and inefficient, while conventional optimization algorithms might get stuck in local minima. To overcome these drawbacks, this study introduced hybrid approach of AI-GOA method to

control the parameters of PID controller. This hybrid approach has several benefits and it is described as follows:

- Integrating the strengths of both algorithms to create a more robust and efficient optimization method.
- Exploration of AO helps identify potential regions, while the gradient guides the search towards the best solution within those regions.
- This synergy can lead to faster convergence, improved robustness, and better overall performance.

3.7.3.1. Aquila Optimizer (AO)

The fundamental formula for the Aquila Optimizer (AO) is provided in this subsection. Frequently, the AO program mimics Aquila's social behaviour in order to capture its prey. The AO has been used to address several issues, including time series forecasting, enhancing global optimization, position scheduling, intrusion detection system (IDS), and other systems. A population-based optimization method is called AO. Eqn. (45) describes how Y is formed using N agents.

$$Y_{ij} = r_1 \times \left(U_j - L_j\right) + L_j, \quad i = (1,2,3,\dots,N);\ j = (1,2,3,\dots,D) \tag{45}$$

Where, the search space is indicated by U_j and L_j; r_1 denotes the interval [0, 1]; D stands for dimension of the solution.

In AO approach, the following step is to either explore or exploit until an optimal solution is found. There are two approaches to exploration and exploitation. The finest agent Y_b and Y_M are utilized in exploration can expressed as follows:

$$Y_i(t+1) = Y_b(t) \times \left(\frac{1-t}{T}\right) + (Y_M(t) - Y_b(t) * rand) \tag{46}$$

$$Y_M(t) = \frac{1}{N}\sum_{i=1}^{N} Y(t), \quad \forall j = 1,2,3,\dots,D \tag{47}$$

Where, the search in Equation (41) is controlled by $\left(\frac{1-t}{T}\right)$; T is the maximum number of generations.

In the meanwhile, the exploration phase uses levy flight $Levy(D)$ to increase population's capacity to identify an optimal solution. This procedure is stated as follows:

$$Y_i(t+1) = Levy(D) \times Y_b(t) + Y_R(t) + (x - y) * rand \tag{48}$$

$$Levy(D) = s \times \frac{\delta \times \tau}{\frac{1}{|v|^{\rho}}} \tag{49}$$

$$\tau = \left(\frac{\Gamma(\rho+1) \times sin\left(\frac{\pi\rho}{2}\right)}{\Gamma\left(\frac{\rho+1}{2}\right) \times \rho \times 2^{\left(\frac{\rho-1}{2}\right)}}\right) \tag{50}$$

Where, the values of ρ and s are set to 0.01 and 1.5 correspondingly. The generation of δ and v is random. A randomly chosen solution from Y is represented by Y_R. Moreover, the parameters y and x represent two that are used to duplicate the spiral shape.

$$x = r \times cos(\theta)\ ; \quad y = r \times sin(\theta) \tag{51}$$

$$r = r_1 + U \times D_1; \quad \theta = -\varepsilon \times D_1 + \theta_1; \quad \theta_1 = \frac{3\pi}{2}; \quad U = 0.005 \tag{52}$$

Where, the random value is denoted by $r_1 \in [0, 20]$.

The first tactic used to enhance the agents in exploitation phase which is analogous to the exploration phase is predicated on Y_b and Y_M, which are expressed as:

$$Y_i(t+1) = \left(Y_b(t) - Y_M(t)\right) \times \alpha - rnd + \left((UB - LB) \times rnd + LB\right) \times \gamma \tag{53}$$

Where, the exploitation parameters are denoted as α and γ.

In the second method of exploitation, Levy, the quality function QF update the position. This method's mathematical definition is as follows:

$$Y_i(t+1) = Y_b(t) \times QF - GY - G_2 \times Levy(D) + rnd \times G_1 \tag{54}$$

$$GY = (Y(t) \times G_1 \times rnd); \quad QF(t) = t^{\frac{2 \times rnd - 1}{(1-T)^2}} \tag{55}$$

Where, the parameter $G_2$is adjusted using the formula that follows. Furthermore, the best solution's mobility is tracked by the parameterG_1, which is updated as follows:

$$G_1 = 2 \times rnd - 1; \qquad G_2 = 2 \times \left(1 - \frac{t}{T}\right) \tag{56}$$

Where, rnd represents a random value.

To increase the accuracy of solution and rate of convergence of GOA algorithm, the update equation is changed by substituting G_1 and G_2 parameters of AO for the random integers r_a andr_b. When it comes to PID control,

especially in non-convex optimization landscapes, AO is particularly good at sifting through the search space and finding a variety of viable solutions. After AO has discovered possible regions, GOA is excellent at local refining and leads the search for the best solutions. Combining these advantages produces a more balanced search that effectively converges to the global optimum while avoiding local minima. The modified update equation of AI-GOA is described in following Eqn. (57).

$$y_y^{m+1} = G_1 \times \left(G_2 \times Y1_y^m + (1 - G_2) \times Y2_y^m\right) + (1 - G_1) \times Y3_y^m \quad (57)$$

4. Results and Discussion

The PV multilevel inverter's nature demands the employment of a high-performance controller whose dynamic responsiveness minimizes error and swiftly reaches the steady state when integrating it into a PV system that is connected to the grid. Three-level algorithms are used in this optimization: Aquila Improved GOA (AI-GOA), Gradient Optimization Algorithms (GOA), and Self-Adaptive-Gradient Optimization Algorithms (SA-GOA). The study utilizes a variety of approaches to assess and compare the performance of three controllers: SA-GOA-PI, AI-GOA-PID, and GOA-FOPI. The circuits are implemented and simulated using MATLAB/Simulink platform.

4.1. Simulink model of proposed circuit

The proposed circuit is generated using Simulink tool. The overall framework model using Simulink is displayed in Fig. 7, Simulink model of buck converter is illustrated in Fig. 8, and the five level inverter Simulink model is displayed in Fig. 9.

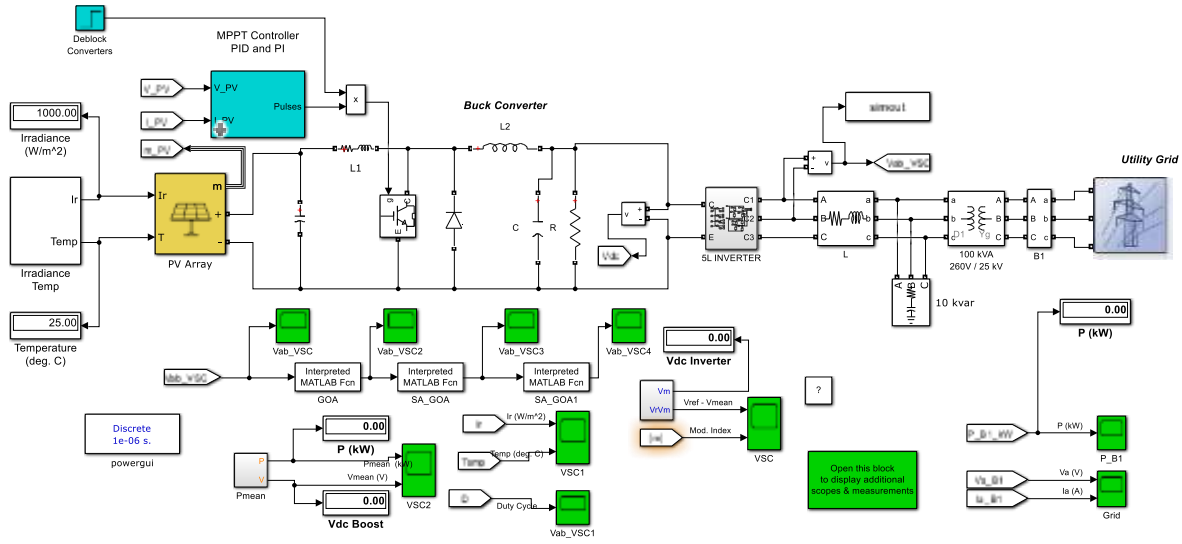

Figure 7. Simulink model of proposed method

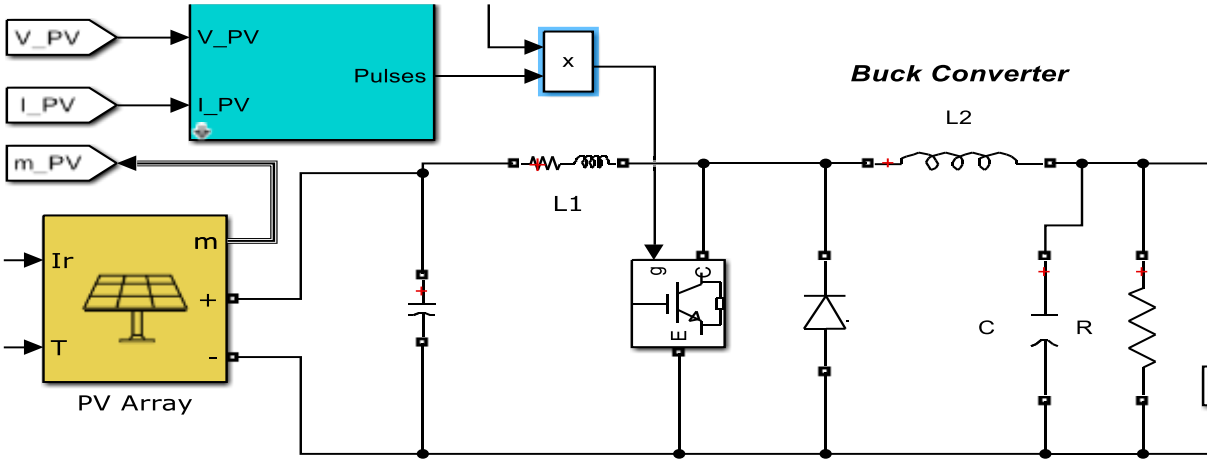

Figure 8. Simulink model of buck converter

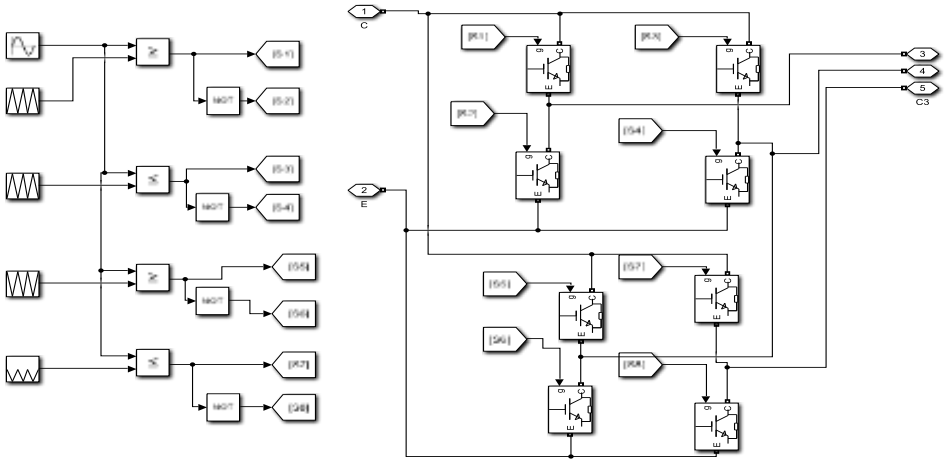

Figure 9. Simulink model of five level inverter

4.2. Simulation Results

A simulation was conducted at a constant ambient temperature of 25°C with varying irradiation conditions to assess the efficacy of the controllers utilized. The applied irradiance was varied between 200 and 1000 W/m^2 in increments of 0.5 seconds. This result is illustrated in Fig. 10.

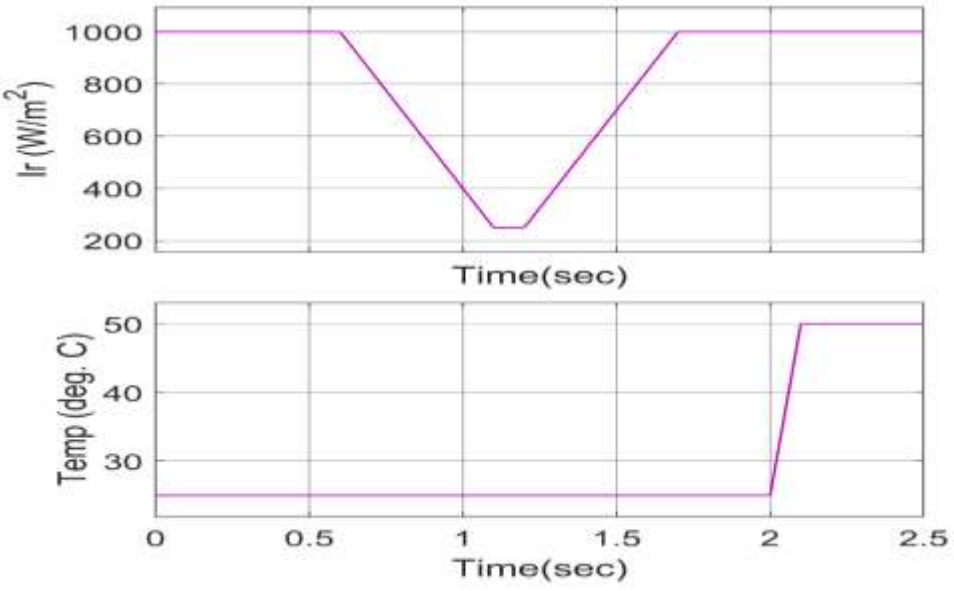

Figure 10. Analysis of Temperature and irradiance

PV diodes are the fundamental components of solar cells. A solar cell's current output usually rises before returning to a steady state level when it is suddenly exposed to light. Initially, MPPT performance is measured experimentally under the presumptions that the PV panels are evenly shadowed and the surrounding air temperature is 25 °C. It is evident that as the irradiance level abruptly drops, the current likewise drops in proportion. Nonetheless, the boost converter keeps the voltage steady. The cell's rise time is the amount of time it takes for the current to reach its steady state level. The PV voltage, current, and diode current analysis is illustrated in Fig. 11. The duty cycle is illustrated in Fig. 12.

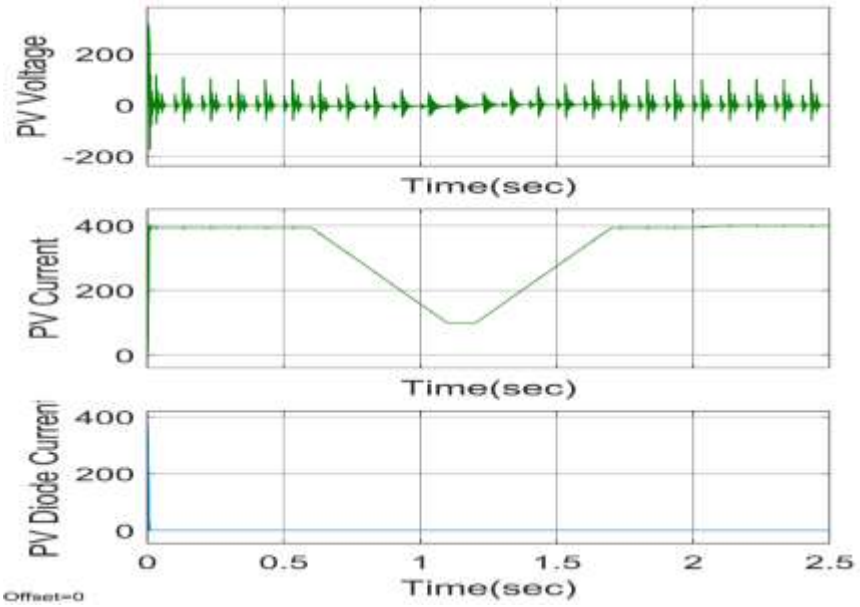

Figure 11. Analysis of PV cells

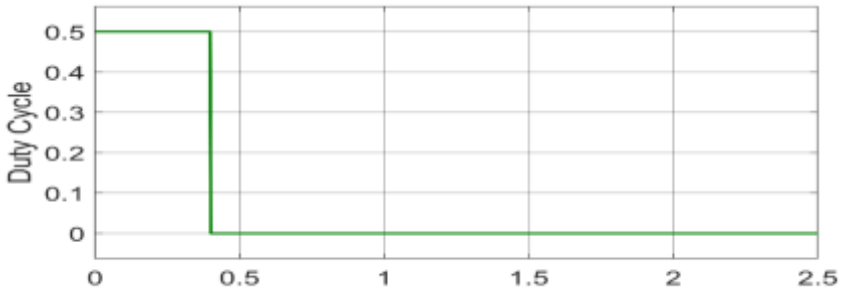

Figure 12. Duty cycle of PV cells

The mean voltage and mean power of five level inverter with three algorithm is displayed in Fig. 13.

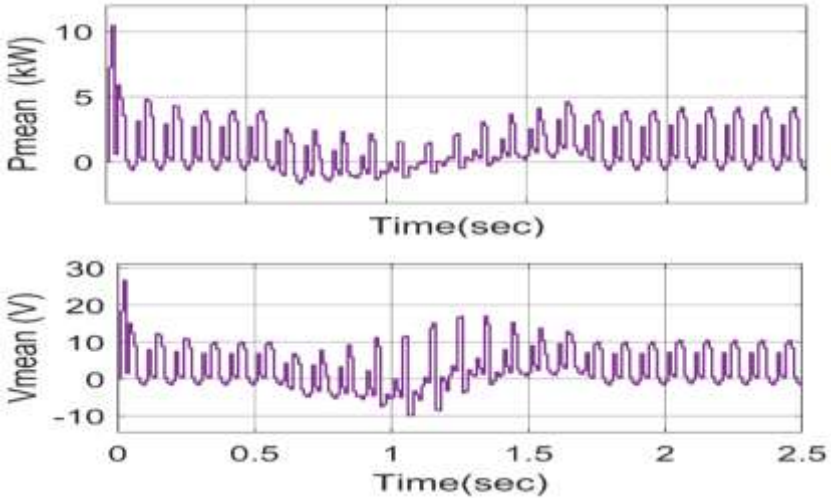

Figure 13. Simulation result of Buck converter

The 5-level inverter receives its input from output of buck converters. Fig. 15 shows the experimental results of power efficiency for the five-level inverter under different output power. The output voltage of the five-level inverter contains five voltage levels. The output voltage with its modulation index and power of the five-level inverter is displayed in Fig. 14.

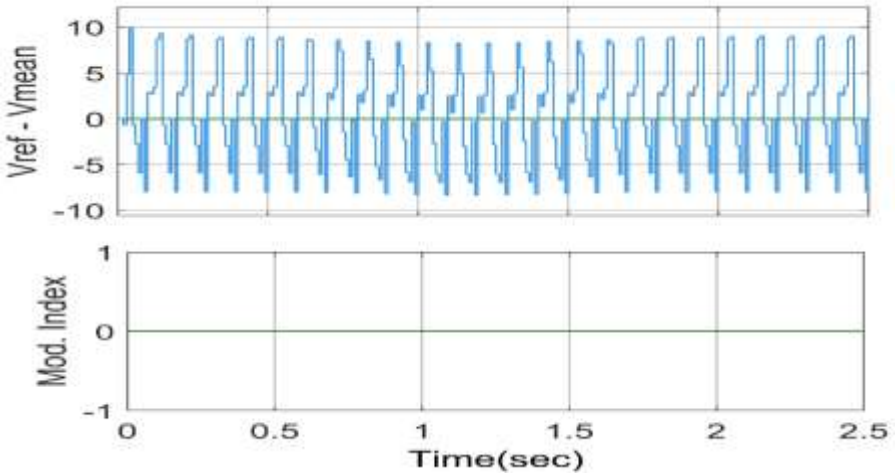

(a) Output voltage of 5 level inverter

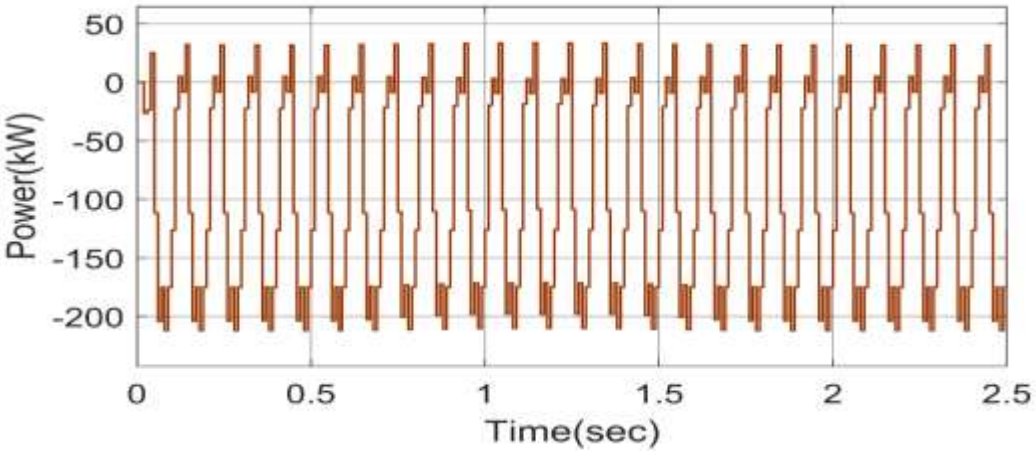

(a) Output power of 5 level inverter

Figure 14. Simulation result of five level inverter

The output voltage, grid voltage, and injected current to the grid are displayed in Fig. 15. The simulation of grid voltage is shown in Fig. 15 (a), and simulation of output voltage and current of grid is illustrated in Fig. 15 (b). It is evident that the grid voltage and the inverter's output voltage are in phase. The apparent power injected into the grid has a constant amplitude, and the phase angle of the injected grid current has undergone a step change.

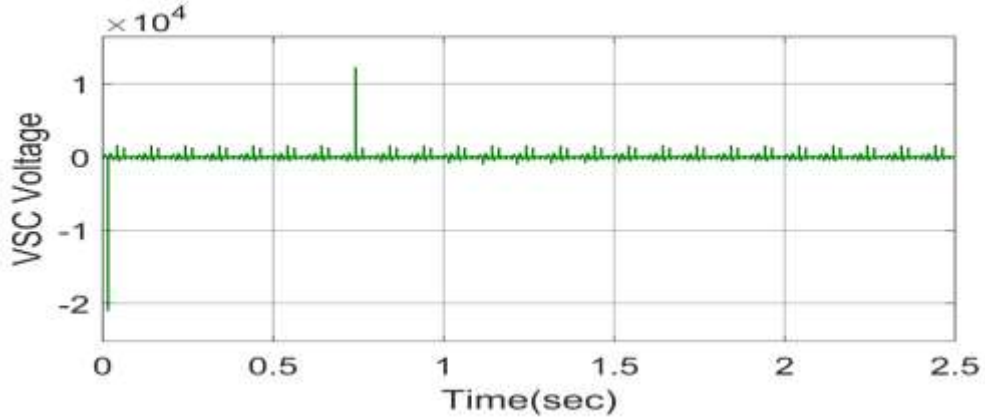

(a) Simulation of grid voltage

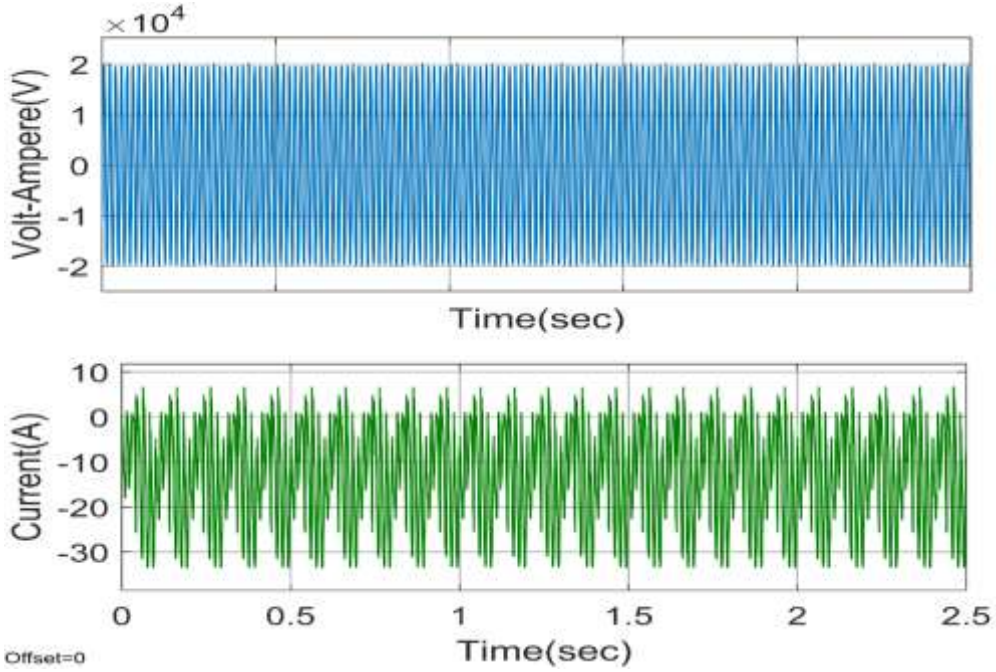

(b) Simulation output voltage and current

Figure 15. Simulation result of grid system

The harmonic spectrum of the injected current to the grid is obtained using MATLAB/Simulink software and shown in Fig. 16 to analyze the Total Harmonic Distortion (THD). The THD of each controller with their metaheuristic algorithm is analysed individually and obtained results are compared with THD of proposed model.

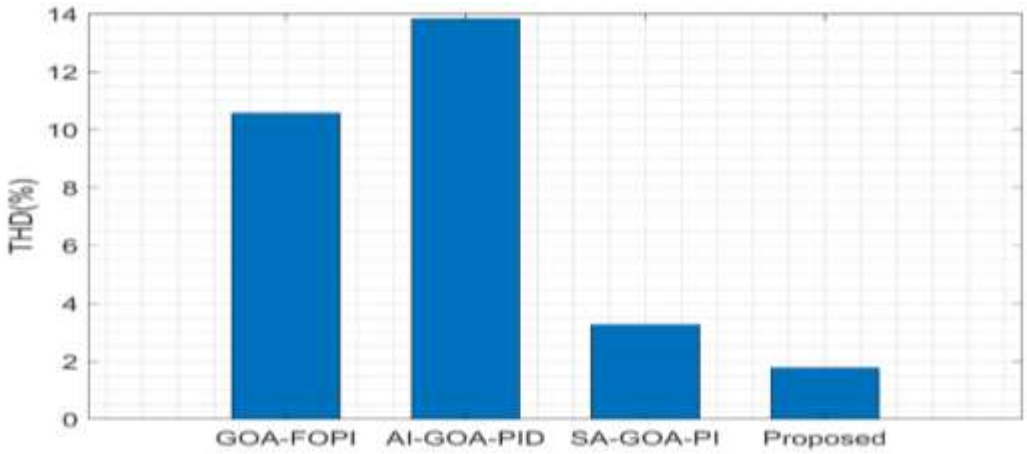

Figure 16. Performance of THD

The THD values of the SA-GOA-PI and AI-GOA-PID systems fall between these two 10.5% and 3% respectively. The GOA-FOPI indicates the highest THD, which is about 14%. The proposed configuration has the lowest THD, which is probably about 2.5%. The aforementioned simulation results demonstrate that the optimal grid may be achieved with the proposed model.

5. Conclusion

This study focuses on improving the dynamic behaviour of grid-connected PV system. The goal is to increase the quality of current injected into the grid and to create a more reliable PV system by enhancing the functionality of control system. Three loops with FOPI, PID, and PI controllers make up the control system. One loop controls the intermediate circuit voltage (Vdc), while the other two loops control the direct and quadratic currents (Ix, Iy) that the multilevel inverter provides. Accurate choice of the controller parameters (Kp, KI, λ) is necessary to increase the multi-level inverter's efficiency and decrease total harmonic distortion (THD) in the output voltage and current. In a similar vein, the Buck converter's PID and PI controller parameters are optimized to improve system performance. To increase the dynamic response of the network-connected PV system, the three controllers' parameters are adjusted using meta-heuristic techniques. Three-

level algorithms are used in this optimization: Aquila Improved GOA (AI-GOA), Gradient Optimization Algorithms (GOA), and Self-Adaptive-Gradient Optimization Algorithms (SA-GOA). The study uses a variety of approaches to assess and compare the performance of three controllers: PI, PID, and FOPI. The values of the parameters of FOPI controllers are adjusted using GOA, PID controller is adjusted by AI-GOA, and PI controller is adjusted using SA-GOA. MATLAB/Simulink software is used to simulate the given model in order to confirm the accurate performance of the proposed system. The simulation results show that the proposed approach may be able to produce the ideal grid.

References

1. Vadavathi AR, Hoogsteen G, Hurink JL. PV Inverter Based Fair Power Quality Control. IEEE Transactions on Smart Grid. 2023 Feb 14.
2. Nkambule MS, Hasan AN, Ali A, Shongwe T. A Novel Control Strategy in Grid-Integrated Photovoltaic System for Power Quality Enhancement. Energies. 2022 Aug 4;15(15):5645.
3. Kanagaraj N, Vijayakumar M, Ramasamy M, Aldosari O. Energy Management and Power Quality Improvement of Hybrid Renewable Energy Generation System Using Coordinated Control Scheme. IEEE Access. 2023 Jul 26.
4. Patel N, Kumar A, Pota HR, Bansal RC, Gupta N. Adaptive qXE-LMF Filter for Improving Power Quality Using Grid-Supporting Photovoltaic System. IEEE Systems Journal. 2023 Feb 22.
5. Hassan A, Bass O, Al-Abdeli YM, Masek M, Masoum MA. A novel approach for optimal sizing of stand-alone solar PV systems with power quality considerations. International Journal of Electrical Power & Energy Systems. 2023 Jan 1;144:108597.
6. Kathiresan AC, Jeyaraj PR, Albert BK, Thanikanti SB, Nallapaneni MK, Alhelou HH. A versatile control of solar DVR for enhanced utilization and power quality improvement in a series-connected wind-solar farm. IET Renewable Power Generation. 2022 Sep 24.
7. Pathak G, Singh B, Panigrahi BK. Multi-operational solar photovoltaic microgrid with synchronization, backup and power quality enhancement ability. e-Prime-Advances in Electrical Engineering, Electronics and Energy. 2023 Sep 1;5:100256.
8. Raziq H, Batool M, Riaz S, Afzal F, Akgül A, Riaz MB. Power quality improvement of a distribution system integrating a large scale solar farm using hybrid modular multilevel converter with ZSV control. Ain Shams Engineering Journal. 2023 Jul 1;14(7):102218.
9. Das S, Singh B. Multi-Objective Control Strategy for Power Quality Improvement in Wind-Solar Distributed Generation System Under Harmonically Distorted Grid. IEEE Transactions on Industry Applications. 2022 Jun 8;58(5):5697-710.
10. Naidu RK, Palavalasa M, Chatterjee S. Integration of hybrid controller for power quality improvement in photo-voltaic/wind/battery sources. Journal of Cleaner Production. 2022 Jan 1;330:129914.
11. Nahin NI, Biswas SP, Mondal S, Islam MR, Muyeen SM. A Modified PWM Strategy With an Improved ANN based MPPT Algorithm for Solar PV Fed NPC Inverter Driven Induction Motor Drives. IEEE Access. 2023 Jun 30.
12. Anguraja R, Sivakumar WM. Power Quality Improvement by Photovoltaic Integrated UPQC-S with Three Level Neutral Point Clamped Diode Inverter Using Modified PQ Theory. InICDSMLA 2020: Proceedings of the 2nd International Conference on Data Science, Machine Learning and Applications 2022 (pp. 1093-1101). Springer Singapore.
13. Kotb KM, Elmorshedy MF, Salama HS, Dán A. Enriching the stability of solar/wind DC microgrids using battery and superconducting magnetic energy storage based fuzzy logic control. Journal of Energy Storage. 2022 Jan 1;45:103751.
14. Masero E, Maestre JM, Camacho EF. Market-based clustering of model predictive controllers for maximizing collected energy by parabolic-trough solar collector fields. Applied Energy. 2022 Jan 15;306:117936.
15. Raziq H, Batool M, Riaz S, Afzal F, Akgül A, Riaz MB. Power quality improvement of a distribution system integrating a large scale solar farm using hybrid modular multilevel converter with ZSV control. Ain Shams Engineering Journal. 2023 Jul 1;14(7):102218.
16. Rao SN, Kumar YV, Pradeep DJ, Reddy CP, Flah A, Kraiem H, Al-Asad JF. Power quality improvement in renewable-energy-based microgrid clusters using fuzzy space vector PWM controlled inverter. Sustainability. 2022 Apr 13;14(8):4663.
17. Prasad D, Dhanamjayulu C. Solar PV-fed multilevel inverter with series compensator for power quality improvement in grid-connected systems. IEEE Access. 2022 Aug 3;10:81203-19.
18. Pidikiti T, Gireesha B, Subbarao M, Krishna VM. Design and control of Takagi-Sugeno-Kang fuzzy based inverter for power quality improvement in grid-tied PV systems. Measurement: Sensors. 2023 Feb 1;25:100638.
19. Reddy SG, Ganapathy S, Manikandan M. Three Phase Four Switch Inverter based DVR for power quality improvement with optimized CSA approach. IEEE Access. 2022 Jul 5;10:72263-78.
20. Alqarni ZA. Design of active fault-tolerant control system for multilevel inverters to achieve greater reliability with improved power quality. IEEE Access. 2022 Jul 25;10:77791-801.

21. Ahmad S, Iqbal A, Ashraf I, Meraj M. Improved power quality operation of symmetrical and asymmetrical multilevel inverter using invasive weed optimization technique. Energy Reports. 2022 Nov 1;8:3323-36.
22. Sanjenbam CD, Shah P, Singh B. Multi-functional control strategy for power quality improvement of three-phase grid using solar PV fed unified power quality conditioner. IET Energy Systems Integration. 2022 Dec;4(4):518-31.